NANOSYSTEMS:
PHYSICS, CHEMISTRY, MATHEMATICS

Original article

Shumigai V.S., et al. *Nanosystems: Phys. Chem. Math.*, 2025, **16** (4), 437–440.
http://nanojournal.ifmo.ru
DOI 10.17586/2220-8054-2025-16-4-437-440

Experimental implementation of multispectral single-pixel imaging in the shortwave infrared frequency range

Vladimir S. Shumigai[1,a], Azat O. Ismagilov[1,b], Anastasiia K. Lappo-Danilevskaia[1,c], Egor N. Oparin[1,d], Anton N. Tcypkin[1,e]

[1]ITMO University, Kronverkskiy, 49, St. Petersburg, 197101, Russia

[a]vshumigay@itmo.ru, [b]ismagilov.azat@itmo.ru, [c]ankonstLD@itmo.ru, [d]en_oparin@itmo.ru, [e]tsypkinan@itmo.ru

Corresponding author: V. S. Shumigai, vshumigay@itmo.ru

ABSTRACT A multispectral single-pixel imaging system operating at three wavelengths – 800 nm, 1050 nm, and 1550 nm – was developed for the imaging of natural materials, such as nuts. Spectral multiplexing of structured illumination patterns was realized using optical elements, and radiation modulation was performed using a digital micromirror device. Data on the integral intensity of the radiation scattered from the object was collected using a collecting lens and one InGaAs photodetector. In accordance with the proposed scheme, images of 25 objects at wavelengths of 800 nm, 1050 nm and 1550 nm were reconstructed. The resolution of the obtained images was 64 by 64 pixels, the time of obtaining one image was about 40 seconds. Experimental results demonstrated the successful reconstruction of images of natural samples exhibiting distinct spectral features, confirming the potential of the system for material characterization and classification.

KEYWORDS single-pixel imaging, short-wave infrared radiation, illumination patterns

ACKNOWLEDGEMENTS This work was supported by the Ministry of Science and Higher Education of the Russian Federation (2025-0007).

FOR CITATION Shumigai V.S., Ismagilov A.O., Lappo-Danilevskaia A.K., Oparin E.N., Tcypkin A.N. Experimental implementation of multispectral single-pixel imaging in the shortwave infrared frequency range. *Nanosystems: Phys. Chem. Math.*, 2025, **16** (4), 437–440.

1. Introduction

Multispectral imaging in the shortwave infrared radiation range (SWIR, 800–1700 nm) is of considerable interest for a variety of applications including agriculture [1], product quality control [2], environmental monitoring and industrial inspection [3]. Since many objects such as moisture, mechanical damage and gases have absorption bands in the SWIR range, the development of devices capable of operating in this frequency range is a current challenge for non-destructive analysis. However, conventional multispectral SWIR cameras have several significant limitations, including high cost due to expensive sensor arrays and the trade-off between resolution, imaging speed and number of spectral channels. The above limitations motivate researchers to develop fundamentally new imaging devices in the SWIR range.

In recent years, single-pixel imaging techniques have attracted attention as an alternative approach for monitoring systems with reduced cost relative to conventional cameras. Unlike matrix detectors, single-pixel imaging systems utilize spatial light modulators and detectors without spatial resolution, thus reducing system cost without significant loss of data quality. One of the key advantages of this method is its flexibility: it can be adapted to operate in different spectral bands, including SWIR, which has been demonstrated in several works. For example, [4] proposed a resolution enhancement method using FSRCNN (fast super-resolution convolutional neural network) combined with Time-of-Flight camera data. However, this approach requires a complex system based on a matrix of laser diodes, which increases the cost and limits the spectral range. Another example [5] uses ghost imaging for methane detection, but at low resolution (16×16 pixels) without applying deep learning. These solutions show that, despite their successes, existing methods either require expensive equipment or do not provide sufficient resolution for detailed analyses. At the same time, the task of implementing full-fledged multispectral imaging in the SWIR range based on single-pixel imaging devices has not yet been solved.

This paper presents several technical solutions for creating a multispectral single-pixel SWIR camera. Unlike the described analogues, the proposed system allows to work with images at several wavelengths of SWIR range, namely at 800 nm, 1050 nm, and 1550 nm. The developed system is oriented on the solution of practical tasks, such as quality control of agricultural products, where it is important to detect hidden defects, or monitoring of industrial processes that require high accuracy.

2. Methodology

As part of the implementation of the single-pixel imaging technique, an object is illuminated by a set of independent illumination patterns. In this work, illumination patterns of 64×64 pixels were generated by rearranging the row elements of the Hadamard matrix H_{4096} (4096×4096 pixels) [6]. The advantages of using such patterns are considered to be their orthogonality, facilitating the extraction of the most complete and independent information about the object during the measurement process, and their binary structure, allowing them to be efficiently reproduced using a digital micromirror device (DMD) without distortion. On the DMD, each pixel corresponded to 12×12 micro-mirrors with a total size of 172.8×172.8 μm. Since the Hadamard matrix values consist of -1 and $+1$, measurements are usually performed using 'positive' and 'negative' patterns, but in this work only the full set of 4096 'positive' Hadamard patterns are used. Provided that using only 'positive' Hadamard patterns does not significantly change the image reconstruction result [7], such a step was taken to halve the measurement time.

To reconstruct the object using the single-pixel imaging technique, it is necessary to obtain the values of integral intensities for each pattern in the experiment. These values correspond to the coefficients of the Hadamard basis decomposition of the object image, from which the spectrum is formed, an example of which is shown in Fig. 1(c). Taking this into account, the reconstruction of the spatial distribution of the object reflection coefficient is performed by the inverse Hadamard transform [8].

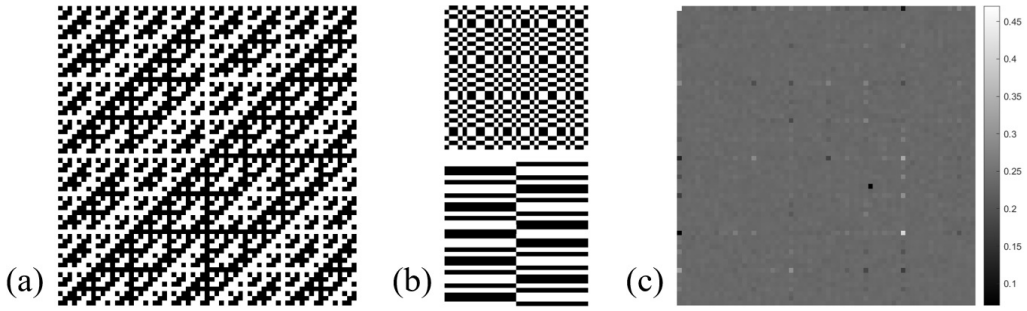

FIG. 1. (a) Hadamard matrix H26, (b) example of illumination Hadamard patterns, 64×64 pixels (c) example of experimental Hadamard spectrum

3. Experimental setup

The experimental implementation of the proposed method is shown in Figure 2. Laser radiation at wavelengths of 800 nm, 1050 nm and 1550 nm is combined into one beam using a system of beam splitter (BS) and mirror at 800 nm (M_{800}). The radiation then enters the beam expander, which consists of a negative lens (L_1) and a positive lens (L_2). After interacting with a DMD with a spatial resolution of 1920 by 1080 pixels and a micro-mirror pitch of 10.8 μm, the radiation at three wavelengths enters the 4f system, which transfers the image from the modulator surface to the objective plane. Moreover, the ratio between the focal length of the first lens f_1 and the focal length of the second lens f_2 are selected so that the illumination pattern increases in size by a factor of 2: from 1 cm on the modulator to 2 cm in the object plane. When interacting with the object, the radiation is scattered to a certain solid angle. Part of this radiation is detected by a detection system consisting of a lens (L_5) and a bucket detector (BD) based on an InGaAs PIN-photodiode with an active area diameter of 1 mm and a wavelength range from 800 nm to 2600 nm. Moreover, the DMD is controlled through a computer, and reading data from BD is done through the analogue-to-digital converter (ADC) LCard E-154 unit connected to the lock-in signal amplifier (LA).

Although the frame switching frequency for the DMD used is 22 kHz, the frequency was reduced to 200 Hz in this work. This was done due to the relatively high value of the LA time constant. For the required gain level, it was 3 ms. Using a wider bandwidth gain will avoid this problem and produce single pixel images at a higher rate.

4. Results

Nuts with enameled paint flecks were considered as the object to be reconstructed. Next, images of 25 objects were reconstructed at each of the SWIR emission wavelengths used, namely at 800 nm, 1050 nm, and 1550 nm. The image reconstruction results for one object are shown in Fig. 3(b-d). The same images after smoothing using median filter are presented in Fig. 3(e-g). Pearson's correlation coefficient (CORR) was used to quantitatively assess the quality of the reconstructed images, considering both the statistical characteristics of the image and its dynamic range [9]. Thus, the average CORR value for 25 objects was 0.61, 0.72, and 0.62 for images reconstructed using wavelengths of 800 nm, 1050 nm, and 1550 nm, respectively.

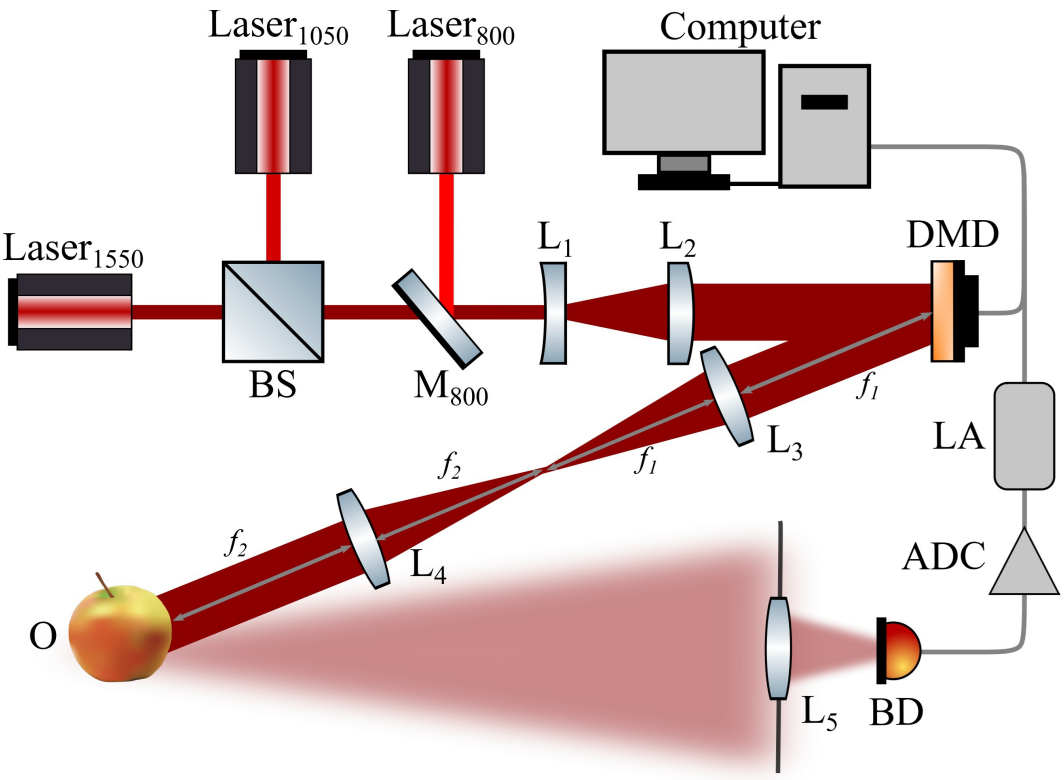

FIG. 2. Experimental setup. BS – beam splitter, M – mirror, L – lens, DMD – digital micromirror device, O – object, BD – bucket detector, LA – Lock-in amplifier.

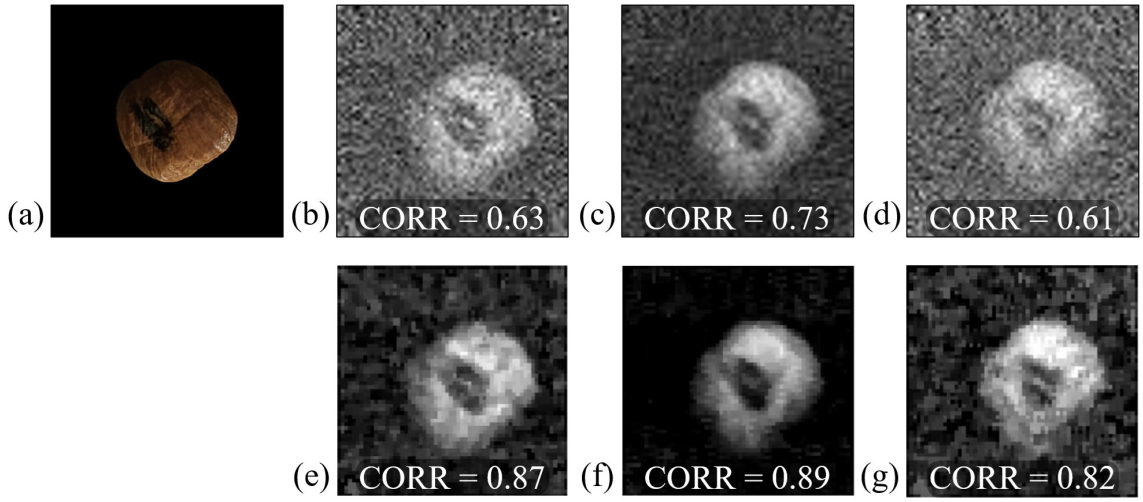

FIG. 3. (a) Image in the visible frequency range; (b)-(d) images reconstructed with the single-pixel imaging algorithm at 800 nm, 1050 nm and 1550 nm, respectively, (e)-(g) image reconstruction with median filter overlay at 800 nm, 1050 nm and 1550 nm, respectively

The highest contrast is achieved for the image at 1050 nm. This takes place because the signal from the single pixel detector for this radiation has the highest signal-to-noise ratio (SNR). For further operation of the system, it is important to realize the same SNR values for the signal in each spectral channel.

5. Conclusion

This paper presents a multispectral single-pixel SWIR-band imaging setup using three spectral channels with central wavelengths of 800 nm, 1050 nm, and 1550 nm. Using the proposed scheme, images of 25 objects with enameled paint flecks absorbing SWIR band radiation were reconstructed. The resolution of the acquired images was 64 by 64 pixels and the acquisition time per image was approximately 40 seconds.

The current implementation of the system requires refinement in several aspects. Firstly, to speed up the operation of the proposed method, it is necessary to use a more broadband amplifier of the detected signal. Second, to improve the contrast of the received images in the detection system, it is necessary to use an objective lens instead of a lens. Thirdly, to realize simultaneous image reconstruction on all three spectral channels, it is necessary to implement spectral-time multiplexing and demultiplexing. Using this technology, it will be possible to fix the integral intensity from three wavelengths at one moment of time.

References

[1] Oliveira R.A., Näsi R., Korhonen P., Mustonen A., Niemeläinen O., Koivumäki N., Honkavaara E. High-precision estimation of grass quality and quantity using UAS-based VNIR and SWIR hyperspectral cameras and machine learning. *Precision Agriculture*, 2024, **25**(1), P. 186–220.

[2] Malakauskas D.M., Ding H., Berman B.P., Thantu N., Karem K.L., Gammino V.M. Shortwave infrared hyperspectral imaging to detect contaminants in the US Food Supply. *Applied Spectroscopy*, 2025, **79**(5), P. 872–878.

[3] Tolentino V., Ortega Lucero A., Koerting F., Savinova E., Hildebrand J.C., Micklethwaite, S. Drone-based VNIR–SWIR hyperspectral imaging for environmental monitoring of a uranium legacy mine site. *Drones*, 2025, **9**(4), P. 313.

[4] Osorio Quero C., Durini D., Rangel-Magdaleno J., Martinez-Carranza J., Ramos-Garcia R. Deep-learning blurring correction of images obtained from NIR single-pixel imaging. *Journal of the Optical Society of America A*, 2023, **40**(8), P. 1491–1499.

[5] Gibson G.M., Sun B., Edgar M.P., Phillips D.B., Hempler N., Maker G.T., Padgett M.J., et.al. Real-time imaging of methane gas leaks using a single-pixel camera. *Optics express*, 2017, **25**(4), P. 2998–3005.

[6] Zhang Z., Wang X., Zheng G., Zhong J. Hadamard single-pixel imaging versus Fourier single-pixel imaging. *Optics Express*, 2017, **25**(16), P. 19619–19639.

[7] Yu Z., Wang X.Q., Gao C., Li Z., Zhao H., Yao Z. Differential Hadamard ghost imaging via single-round detection. *Optics Express*, 2021, **29**(25), P. 41457–41466.

[8] Wang L., Zhao S. Fast reconstructed and high-quality ghost imaging with fast Walsh–Hadamard transform. *Photonics Research*, 2016, **4**(6), P. 240–244.

[9] Cohen I., Huang Y., Chen J., Benesty J., Benesty J., Chen J., Cohen I. *Pearson correlation coefficient*. In: Noise Reduction in Speech Processing, 2009, Berlin: Springer, P. 1–4.

Submitted 28 May 2025; revised 11 June 2025; accepted 12 June 2025

Information about the authors:

Vladimir S. Shumigai – ITMO University, Kronverkskiy, 49, St. Petersburg, 197101, Russia; ORCID 0000-0001-8597-1196; vshumigay@itmo.ru

Azat O. Ismagilov – ITMO University, Kronverkskiy, 49, St. Petersburg, 197101, Russia; ORCID 0000-0002-5844-2966; ismagilov.azat@itmo.ru

Anastasiia K. Lappo-Danilevskaia – ITMO University, Kronverkskiy, 49, St. Petersburg, 197101, Russia; ORCID 0000-0002-1762-2688; ankonstLD@itmo.ru

Egor N. Oparin – ITMO University, Kronverkskiy, 49, St. Petersburg, 197101, Russia; ORCID 0000-0002-4009-7594; en_oparin@itmo.ru

Anton N. Tcypkin – ITMO University, Kronverkskiy, 49, St. Petersburg, 197101, Russia; ORCID 0000-0002-9254-1116; tsypkinan@itmo.ru

Conflict of interest: the authors declare no conflict of interest.